JM PAPERS

Observations of transient wave-induced mean drift profiles caused by virtual wave stresses in a two-layer system

Jan Erik H. Weber[1,†], Yiyi Whitchelo[2], Jon A. Pirolt[2],
Kai H. Christensen[1,3], Jean Rabault[3] and Atle Jensen[2]

[1]Department of Geosciences, University of Oslo, PO Box 1022, Blindern, NO-0315 Oslo, Norway

[2]Department of Mathematics, University of Oslo, PO Box1053, Blindern, NO-0316 Oslo, Norway

[3]Norwegian Meteorological Institute, PO Box 43, Blindern, NO-0313 Oslo, Norway

An experimental study of long interfacial gravity waves was conducted in a closed wave tank containing two layers of viscous immiscible fluids. The study focuses on the development in time of the mean particle drift that occurs close to the interface where the two fluids meet. From a theoretical analysis by Weber & Christensen (*Eur. J. Mech.*-B/*Fluids*, vol. 77, 2019, pp. 162–170) it is predicted that the growing drift in this region is associated with the action of the virtual wave stress. This effect has not been explored experimentally before. Interfacial waves of different amplitudes and frequencies were produced by a D-shaped paddle. Particle tracking velocimetry was used to track the time development of the Lagrangian mean drift. The finite geometry of the wave tank causes a mean return flow that is resolved by mass transport considerations. The measurements clearly demonstrate the importance of the virtual wave stress mechanism in generating wave drift currents near the interface.

Key words: internal waves

1. Introduction

Longuet-Higgins ([1953](#)) extended the result of Stokes ([1847](#)) of mean drift in irrotational surface gravity waves (known as the Stokes drift) to fluids with viscosity. The effect of viscosity causes damping of the wave field such that some mean wave momentum is transferred to Eulerian mean currents. This transfer is achieved by the action of the virtual

wave stress (VWS) at the surface (Longuet-Higgins 1969). The VWS is the manifestation of mean vorticity being generated in the oscillatory boundary layer, and it depends solely on the linear wave solutions and the rheological properties of the surface. If the surface is covered by a thin film, the VWS is greatly enhanced, and the wave-induced Eulerian mean currents become stronger than the Stokes drift in a relatively short time interval (Christensen & Weber 2005). From vorticity considerations, the increased drift in the case of an inextensible film cover was originally derived by Craik (1982).

A closed tank is typically used in a laboratory setting, with a wave maker mounted at one end, and with wave energy absorbing materials at the other end. For a one-layer system with a free surface, the VWS at any specific point will be constant in time as soon as the first wave front has traversed the full length of the tank. With a constant flux of mean momentum from the waves to the mean flow, the mean wave-induced drift currents will increase in time and space by diffusion (Longuet-Higgins 1953; Weber 2001). Eventually, a steady state will be reached when the VWS is balanced by the viscous stresses at the bottom and at the tank walls.

A similar effect occurs for interfacial gravity waves in a two-layer system; see for example Weber & Christensen (2019), hereafter referred to as WeCh. However, theoretical studies of the drift in gravity waves in a two-layer setting with different viscosities and densities are not new. In an Eulerian formulation this problem was studied by Dore (1970, 1973, 1978*a*,*b*) and Wen & Liu (1995). Furthermore, Weber & Førland (1990), Piedra-Cueva (1995) and Ng (2004) applied a direct Lagrangian formulation to this problem.

Numerous experimental studies have also been conducted on drift trajectories in a two-layer system. For example, the work of Sakakiyama & Byker (1989) investigated the mass transportation in a mud layer. The work of Grue *et al.* (2000) investigated the effect of breaking and mass transport in layers of salt water with different densities, while Umeyama & Matsuki (2011) studied the trajectory of wave particles in a two-layer salt–fresh water system.

So far, the majority of the experimental studies on mass transport have been conducted with two layers of miscible fluids. As such, miscible fluids cannot maintain a sharp discontinuous density gradient at the interface (Weber, Christensen & Broström 2014), and the effect of diffusion and mixing will quickly take place in the case of large-amplitude waves. This makes it difficult to measure the Lagrangian mean drift close to the interface.

For this reason, the experiments we present in this paper were performed using Isopar V, produced from petroleum-based raw materials, and fresh water, constituting two immiscible fluids. The conducted experimental study aims at verifying the theoretical results by WeCh, focusing on the existence of VWS and the time development of a mean drift in interfacial waves.

There are two obvious problems that occur when we compare idealized theory with laboratory experiments. They are basically related to the finite geometry of the wave flume. First, for linear theory, the spatial damping of interfacial waves becomes larger in the tank due to the viscous effects of sidewalls and rigid top and bottom planes; see e.g. the discussion by Troy & Koseff (2006). Second, when nonlinear theory is concerned, the finite geometry of the wave flume will induce a return flow opposing the Lagrangian mean drift in the wave propagation direction. We discuss this in connection with the presentation of the experimental results. The rest of the paper is organized as follows: in § 2 we recapitulate the theoretical results in WeCh, and in § 3 we describe the experimental set-up. In § 4 we present the experimental results, while § 5 compares the experimental results with theory. Furthermore, § 6 considers the effect of the VWS, while § 7 contains a discussion and some final remarks.

2. Theory

For details of the theory on the Lagrangian mean drift in long interfacial gravity waves, we refer to WeCh. The results in that paper are based on weak nonlinear theory for small-amplitude interfacial waves in an infinitely long channel with no vertical boundaries. Upper and lower fluids are immiscible, incompressible and viscous. The waves are long compared with the depth of the two layers, and the hydrostatic assumption has been made in the vertical. Viscous effects of the upper (top) and lower (bottom) boundaries have been neglected. It is important to have these points in mind when we later compare the observed Lagrangian mean drift in a finite-length laboratory wave tank with the theory in WeCh.

In the following, we state the main results that will be useful when comparing with the laboratory measurements reported in the coming paragraphs. Analogous to the one-layer case with a free surface, the Lagrangian mean drift velocity u_L in spatially damped waves is composed of a (basically irrotational) Stokes drift u_S, a time-independent viscous boundary-layer solution u_B (sometimes referred to as the boundary-layer 'steady streaming') and an Eulerian mean current u_E. The last quantity develops in a diffusive manner in space and time because $u_S + u_B$ does not fulfil the boundary condition at the common interface. In this way, the initial mean wave momentum is transferred to Eulerian mean currents; see Longuet-Higgins (1953).

We consider two horizontal layers of immiscible incompressible viscous fluids. The undisturbed layer depths are H_1 and H_2 with densities ρ_1 and ρ_2 ($\rho_2 > \rho_1$), where subscripts 1 and 2 refer to the upper and lower layers, respectively. The corresponding viscosities are ν_1 and ν_2. We place the x-axis along the undisturbed interface and the z-axis vertically upwards. As first shown by Longuet-Higgins (1969), the condition at the boundary that drives u_E can be expressed as a so-called VWS, denoted by τ_w. We here concentrate on the development of the drift current near the interface. In this case, we have by definition that

$$\tau_{w1,2}/\rho_{1,2} = \nu_{1,2}\partial u_{E1,2}/\partial z, \quad z = 0. \tag{2.1}$$

It should be pointed out that, although the VWS is derived from quantities that are continuous at the interface (velocity and viscous stress), the VWS itself is not continuous.

The results in WeCh are derived by using Lagrangian particle-following coordinates. In the formulas for the mean flow quoted here, we can, to leading order, simply replace them by the independent Eulerian coordinates (x, z). Thus, we have in the two layers that

$$u_{L1,2} = u_{S1,2} + u_{B1,2} + u_{E1,2}, \tag{2.2}$$

where the Stokes drift can be written

$$u_{S1} = cA^2 \exp(-2\alpha x)/(2H_1^2), \tag{2.3}$$

$$u_{S2} = cA^2 \exp(-2\alpha x)/(2H_2^2). \tag{2.4}$$

Here, $c = \omega/k$ is the phase speed, where ω is the angular frequency and k the wavenumber. Furthermore, α is the spatial wave damping rate, and A is the interfacial wave amplitude at the horizontal position $x = 0$.

The steady streaming in the viscous boundary layers near the interface becomes

$$u_{B1} = u_{S1}Q_1[\tfrac{3}{2}Q_1 \exp(-2\gamma_1 z) - 4\exp(-\gamma_1 z)\cos(\gamma_1 z)], \tag{2.5}$$

$$u_{B2} = u_{S2}Q_2[\tfrac{3}{2}Q_2 \exp(2\gamma_2 z) - 4\exp(\gamma_2 z)\cos(\gamma_2 z)], \tag{2.6}$$
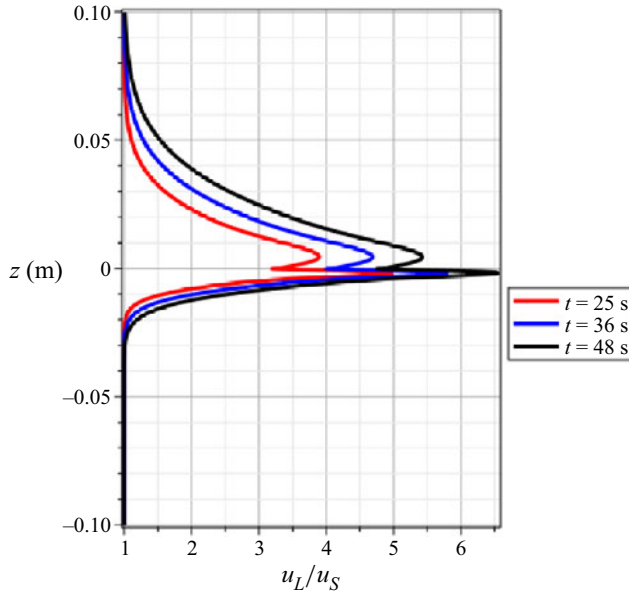
Figure 1. Non-dimensional Lagrangian wave drift solutions as function of height from WeCh at various times t. Here, $u_{S1} = u_{S2} = u_S$.

where $\gamma_{1,2} = [\omega/(2\nu_{1,2})]^{1/2}$. The order of magnitude of the viscous boundary-layer thicknesses is

$$\delta_{1,2} = 1/\gamma_{1,2}. \tag{2.7}$$

Introducing $R = 1/(1 + r)$, where $r = \nu_2^{1/2}/\nu_1^{1/2}$, we can write the constants in (2.5) and (2.6) as

$$Q_1 = (H_1 + H_2)(1 - R)/H_2, \tag{2.8}$$

$$Q_2 = (H_1 + H_2)R/H_1. \tag{2.9}$$

Finally, the Eulerian mean drift currents can be written

$$u_{E1} = -u_{S1}R[rF\,\mathrm{erfc}(X_1) - G(2\omega t)^{1/2}\,\mathrm{ierfc}(X_1)], \quad z \geq 0, \tag{2.10}$$

$$u_{E2} = -u_{S1}R[F\,\mathrm{erfc}(-X_2) + G(2\omega t)^{1/2}\,\mathrm{ierfc}(-X_2)], \quad z \leq 0, \tag{2.11}$$

where $X_{1,2} = z/(4\nu_{1,2}t)^{1/2}$. The constants here are given by

$$F = (1 + h)[(3 + r)h - 1 - 3r]/(2 - 2r), \tag{2.12}$$

$$G = r(1 + h)^2/(1 + r), \tag{2.13}$$

where $h = H_1/H_2$.

Parameters relevant for the experiments with small amplitudes described in this paper with Isopar V ($\nu_1 = 1.44 \times 10^{-5}\ \mathrm{m^2\ s^{-1}}$) above water ($\nu_2 = 1.12 \times 10^{-6}\ \mathrm{m^2\ s^{-1}}$) are $H_1 = H_2 = 0.1$ m, $\omega = 2.2\ \mathrm{s^{-1}}$, $k = 7.57\ \mathrm{m^{-1}}$ and $A = 0.0102$ m. For later reference, we depict in figure 1 the transient non-dimensional Lagrangian wave drift solutions in both layers after 25, 36 and 48 s from WeCh for this set of parameters.

Actually, the laboratory experiments, which we discuss later on in § 4, were performed for a wider range of amplitudes and frequencies than those used to construct figure 1; see

975 A12-4

Pirolt ([2021](#)). However, for comparison with the weakly nonlinear theory in WeCh, the selected experimental amplitudes had to be as small as possible for waves in the long wave regime.

In WeCh it was demonstrated that, through the action of the VWS defined by (2.1), the induced Eulerian mean currents (2.10)–(2.11) exhibited a pronounced jet-like structure near the interface, as seen in figure 1. For times larger than zero, using that $H_1 = H_2$, we find from (2.10) for the upper layer

$$u_{E1} = 2u_{S1}r[4(t/T)^{1/2} + r - 1]/(1 + r)^2, \quad z = 0, \tag{2.14}$$

where T is the wave period. A similar result is obtained for the lower layer. Hence, the Eulerian mean currents at the interface increases in time proportional to $(t/T)^{1/2}$.

3. Experimental methodology

The experiments were performed in a wave tank located in the Hydrodynamics Laboratory of the University of Oslo. The dimensions of the tank are 7.3×0.25 m (length × width). A beach, made out of a synthetic grass material similar to what is used for sports fields, was used to dampen the waves at the end of the tank. The beach was inclined at an angle of $10°$ and intercepted the full depth of the fluid layers. We found that the beach reflected a maximum 10 % of the incoming wave energy for the longest waves ($\lambda = 0.83$ m) and down to below 3 % for the shorter waves. In the experiments, we have used fresh water ($\rho_2 = 998$ kg m^{-3}) for the bottom layer, and Isopar V ($\rho_1 = 815$ kg m^{-3}) for the top layer. The density of the fluids was checked using a laboratory rheometer under the environmental conditions of the experiments (temperature around 20 °C). In all the following, the thickness of bottom layer was kept constant at 10 cm and the top layer at 10 or 20 cm. For details of the paddle design and wave generation, we refer to Pirolt ([2021](#)). Rigid lids made of Styrofoam were placed on top of the Isopar V layer and secured in place with a steel frame clamped on the wave tank. This was done in order to suppress the generation of surface waves due to paddle motion. The model and the experimental set-up are sketched in figure 2(*a,b*).

Camera locations 1 and 2 were positioned at approximately 1 and 3 m distance from the wave maker. Each location was equipped with two AOS PROMON U750 MONO cameras, one upper camera for the Isopar V layer and one lower camera for the water layer. The cameras were tilted at an angle of maximum $\pm 10°$ to avoid capturing the area where the Isopar V adheres to the glass wall of the tank (leading to blurred regions in the images) whilst also focusing on the water–Isopar V interference site. The distortion of the image captured due to this angle was considered in the 'pixel to world' coordinates by using a cubic transform. Each camera has a resolution of 1280×1024 pixels, which correspond to 1 pixel $= 0.01$ mm, and the experimental images were captured at a frame rate of 50 f.p.s.

The mid-plane of the water column at each location was illuminated with a LED light sheet placed below the transparent base of the tank. Each LED light sheet had a thickness of approximately 1.5 cm and it illuminated a section of the tank around 0.5 m long. The side of the tank on the opposite side to the cameras was covered with black (non-reflective) paper so the background of the laboratory would not interfere with the visualization of the wave motion in the tank.

For a general run, the water layer and Isopar V layers were seeded separately with polyamide particles with diameters 50 and 100 μm. The particles have a density of 1.03 g cm^{-3} and were found to be almost neutrally buoyant in both fluids. The fluids were
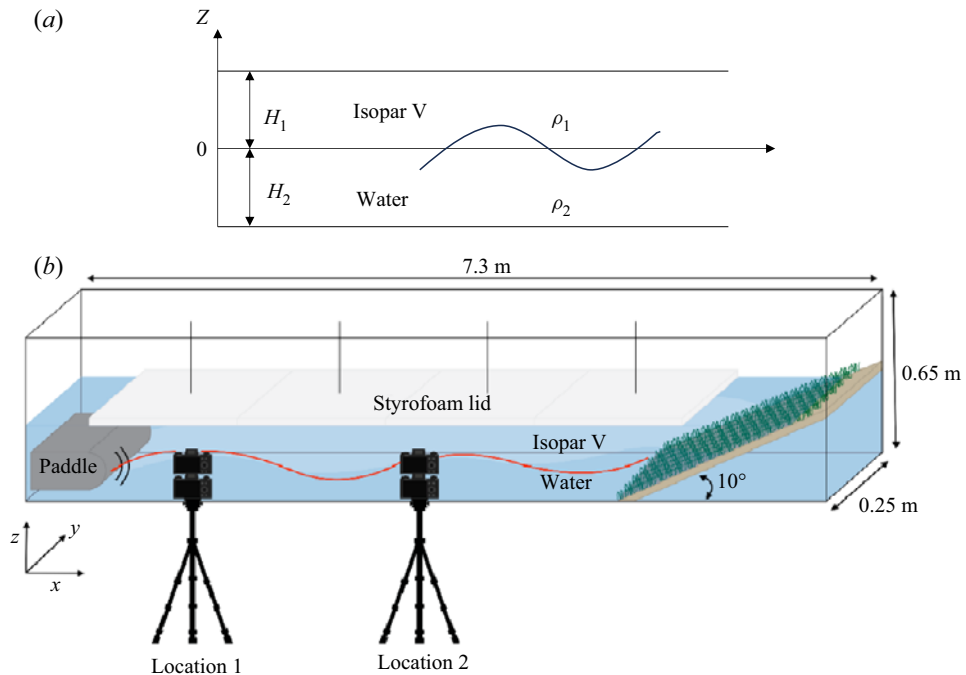
Figure 2. (*a*) Conceptual sketch of fluid model with two immiscible fluids. The lighter fluid, Isopar V, resides at the top and water at the bottom. (*b*) Illustration of the wave tank. A half-ellipsoid wave paddle was attached at one end of the tank and a beach inclined at 10° was placed at the opposite end. Camera locations 1 and 2 were used for the PTV measurements.

then gently stirred and sufficient time was allowed for the fluid motion to halt, securing a homogeneous particle distribution in the tank.

The paddle generated monochromatic waves that propagated down the length of the tank. The wave characteristics were measured by using image processing in MATLAB. First, we constructed a time series image from selecting the same pixel column of each image in an experimental run. The interface was identified by light reflecting from the passive particles that gathered on the surface of the water layer, forming a distinctive high luminosity line at the interface between the fluids. Then, from the time series images, a script was run to trace the middle of the interface light line and then transform the distorted instantaneous coordinates into reference world coordinates. Finally, we extracted the amplitude and frequency for each experiment.

For the particle tracking velocimetry (PTV) analysis, the images from an experimental run were first pre-processed to mask out the unused regions. Then, a PTV analysis was used to measure the instantaneous Lagrangian mean drift at the so-called end of each period, so that the interface lies at its reference height. The program uses blob tracking to identify each particle and track it for each period in DigiFlow (Dalziel 2006). The Lagrangian mean drift is then calculated by measuring the distance between the start and end of a successful trace and dividing it by the period.

The boundary-layer thickness is difficult to measure experimentally. In the experiments, δ_1 and δ_2 defined by (2.7) were 0.004 and 0.001 m, respectively. One possible way is to analyse the shape of the Lagrangian mean drift from PTV tracking. However, the PTV measurements have a tendency to miss the particles very close to the interface. One reason is related to the mean z-position of the particle path, which is the centre of the particle trajectory for a given period. Given our experimental images, the program will fail to track
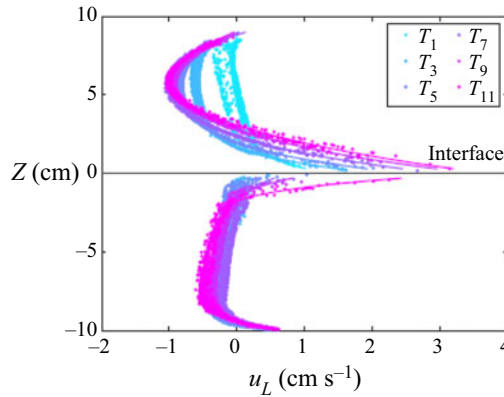
Figure 3. Lagrangian drift velocity as a function of height for successive periods T_n. Here, $H_1 = H_2 = 0.1$ m, $\omega = 2.2$ s^{-1} and $A = 0.0148$ m. The solid lines are the best fit to the scattered data points, yielding the Lagrangian mean flow as a function of height.

any particles that blurred into the interface shine by the LED light sheet. Another reason could be that the particles travel out of the field of view, leading to insufficient tracking for a whole period, which is needed for calculating the Lagrangian mean drift. Consequently, the subtle difference between the Eulerian and Lagrangian mean positions of the material interface, as discussed in WeCh, could not be detected.

4. Experimental results

First, we give a qualitative overview of the experimental results in both layers. For this purpose, we choose data from camera location 2, with frequency $\omega = 2.2$ s^{-1}, and amplitude $A = 1.48$ cm. Figure 3 depicts the vertical variation of the Lagrangian mean drift for successive periods in this case.

We notice the qualitative resemblance between the theoretical results, as depicted in figure 1, and the experimental results in figure 3. Especially, we remark the pronounced jet-like behaviour of the drift current near the interface. However, we also note the return flow in the experiments, which is not accounted for by the theory. In WeCh, it was assumed that the wave channel was infinitely long with no vertical walls that could obstruct the horizontal mean flow. In the laboratory, on the other hand, we have a finite-length wave tank that is closed at both ends. Accordingly, as soon as the wave field is established throughout the length of the tank, there must be a negative mass flux balancing the positive wave-induced Lagrangian flux in each layer.

As seen in figure 3, the development of the drift current in time and space is qualitatively the same in both layers. However, it was somewhat problematic to process the data from the (lower) water layer. In many cases, we did not get close enough to the interface to observe the steady streaming, and overall, the tracking did not give a consistent, repeatable result. In conclusion, we find that the camera resolution was insufficient to produce high quality PTV tracking in the lower layer. For a quantitative comparison with the theoretical results, we therefore concentrate on the data from the (upper) oil layer, where the processing was easier.

4.1. *Upper-layer measurements*

The theoretical results in WeCh are valid for small-amplitude waves, where $A/H_{1,2} \ll 1$. The experimental parameter set that comes closest to the assumptions in the theory (used
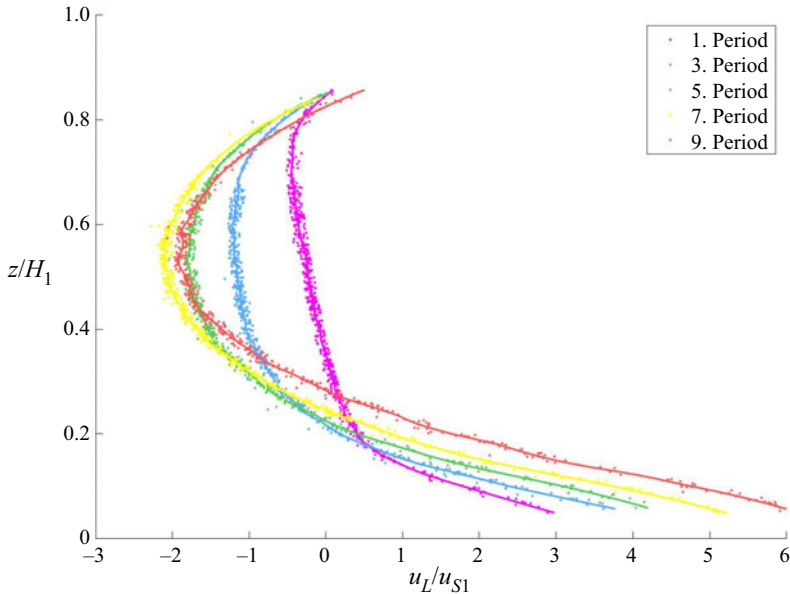
Figure 4. Experimental Lagrangian drift results for the upper layer (dotted points) for successive periods when $H_1 = H_2 = 0.1$ m, $\omega = 2.2$ s^{-1}, $k = 7.57$ m^{-1} and $A = 0.0102$ m. The solid lines are the best fit to the scattered data points, yielding the Lagrangian mean flow as a function of height at various times.
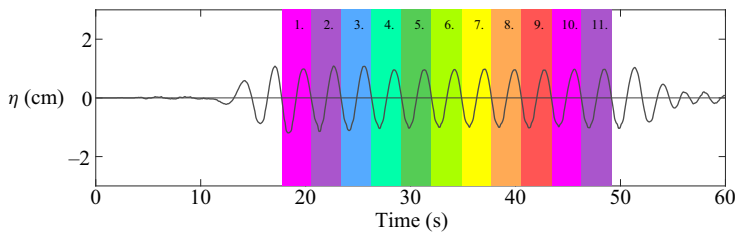

Figure 5. Time series showing chosen periods for the plotted data in figure 4. Here, η is the interfacial elevation at camera position 2.

to construct figure 1) is $H_1 = H_2 = 0.1$ m, $\omega = 2.2$ s^{-1}, $k = 7.57$ m^{-1} and $A = 0.0102$ m at camera location 2. The Lagrangian measurements of the upper-layer mean drift in this case are depicted in figure 4.

In the regions close to the interface (inside the viscous boundary layer) and in the viscous region near the upper rigid boundary, reliable measurements could not be obtained. This explains the lack of data points in the figure.

In figure 5, we have displayed the interfacial elevation as function of time. Periods and colour codes correspond to those in figure 4.

Again, it is particularly interesting to note the increase in time of the Lagrangian drift velocity close to the interface in figure 4. This is a strong indication that the Lagrangian drift develops in the manner predicted by the theory of WeCh; see e.g. figure 1. For a quantitative comparison, we have to adjust for the return flow in the tank, which is an obvious feature in figures 3 and 4. This will be attempted in § 5.

975 A12-8

5. Comparison with theory

To compare the experimental results with the theory in WeCh, we must quantify the return flow in the experiments seen in figures 3 and 4. As discussed in § 4, volume conservation in the upper layer requires that

$$\int_0^{H_1} (u_{L1} + u_{R1})\, \mathrm{d}z = 0, \tag{5.1}$$

where u_R is the return flow. For continuity reasons, this relation must be valid at any horizontal position down the tank. The corresponding return flux becomes

$$U_{R1} \equiv \int_0^{H_1} u_{R1}\, \mathrm{d}z = -\int_0^{H_1} u_{L1}\, \mathrm{d}z. \tag{5.2}$$

Obviously, this flux varies with time. As a first approximation, we take that the return flow is parabolic. This is the simplest form that yields a net transport while satisfying the top and bottom no-slip boundary conditions in the tank. The parabolic approximation has previously been observed to provide good agreement with wave tank experimental flow profiles (Rabault *et al.* 2016). From the observations, we note a return flow maximum near the middle of each layer. Hence, we assume

$$u_{R1} = K_1 z(z - H_1). \tag{5.3}$$

We then find for the time-dependent coefficient that

$$K_1 = -6U_{R1}/H_1^3, \tag{5.4}$$

where U_{R1} is given by (5.2). However, it should be remarked from the experimental data presented in figure 4 that, for small times (first period), the parabolic form of the return flow is not very well developed, while for longer times the profile shows a much more parabolic behaviour.

In figure 6, we have depicted the theoretical result u_L/u_{S1} from (2.2) by adding the model result u_{R1}/u_{S1} from (5.3). In the same figure, we have replotted the experimental data for the Lagrangian drift shown in figure 4. The vertical plot range in the figure is limited to the region where we have reliable measurements, i.e. between the viscous boundary layers at the interface and at the top.

From the results presented in figure 6, we conclude that the theory in WeCh, with the added return flow, reproduces the experimental results quite well. This is particularly so for larger times when the return flow in the wave tank becomes more parabolic.

Finally, apart from the assumption of an idealized parabolic profile, it should be pointed out that the observed discrepancy between experiments and theory also could be caused by nonlinear effects not taken into account here.

6. Virtual wave stress

The basic intention behind the present laboratory investigation is to verify the strong transfer of mean momentum from interfacial waves to jet-like mean drift currents near the interface, as predicted by the theory in WeCh. The action of VWS at the interface is central in this theory. As explained before, we have difficulties in measuring the steady streaming u_B in the viscous boundary layer, which is part of the Lagrangian velocity. But this is not crucial for the present investigation, since we are basically interested in the wave-induced Eulerian mean current, or, more specifically, the spatial gradient $\partial u_E/\partial z$, which determines the VWS.
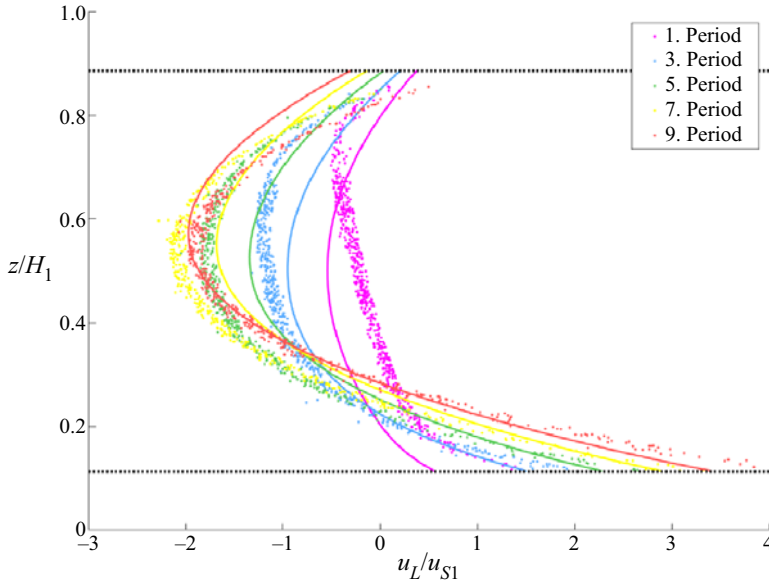
Figure 6. The experimental Lagrangian drift data from figure 4 displayed together with the theoretical result (2.2) of WeCh (solid lines), when the return flow (5.3) is added. The horizontal dotted lines mark the outer end of the viscous boundary layers (thickness $\pi\delta_1$) at the interface and at the top.

In the upper layer, we find from (2.10) that the VWS can be written

$$\tau_{w1}/\rho = \nu_1(\partial u_{E1}/\partial z)_{z=0} = u_{S1}\nu_1^{1/2}R[rF/(\pi t)^{1/2} - G\omega^{1/2}/2^{1/2}], \qquad (6.1)$$

where the constants are given by (2.12) and (2.13). It is not possible to compare (6.1) directly with the experimental results, since we only measure the Lagrangian drift for $z \geq \delta_1$. However, outside the viscous boundary layer, we have that $\partial u_{E1}/\partial z \approx \partial u_{L1}/\partial z$. This fact can be used when we compare experimental gradients with theory.

In the measurements, the Lagrangian mean flow gradients are affected by the shear of the return flow. For a direct comparison, we must add our parabolic flow (5.3), constructed to yield zero net mass transport in the upper layer. The result is shown in figure 7, where we have compared the mean drift gradients at the edge of the viscous boundary layer.

We emphasize that there are uncertainties related to the determination of spatial gradients from the data, and also to the vertical position at which theory and measurements should be compared. However, generally, the computed gradients are of the same order of magnitude in the theory and the measurements, and so are their variation in time. We therefore conclude that the correspondence between the theoretical and measured drift gradients seen in figure 7, demonstrates that the VWS mechanism can generate such wave drift currents as we observe near the interface in the wave tank.

7. Discussion and concluding remarks

We have performed laboratory experiments in a closed wave tank containing two layers of immiscible fluids. A D-shaped paddle produced interfacial waves of different frequencies and amplitudes. Four cameras, two at each measurement location in the tank, were used to capture the fluid flow motion. We used PTV measurements to determine the instantaneous Lagrangian mean drift velocity u_L. An increase in u_L close to the interface was observed as time progressed, just as predicted by the theory of WeCh. The finite geometry of the
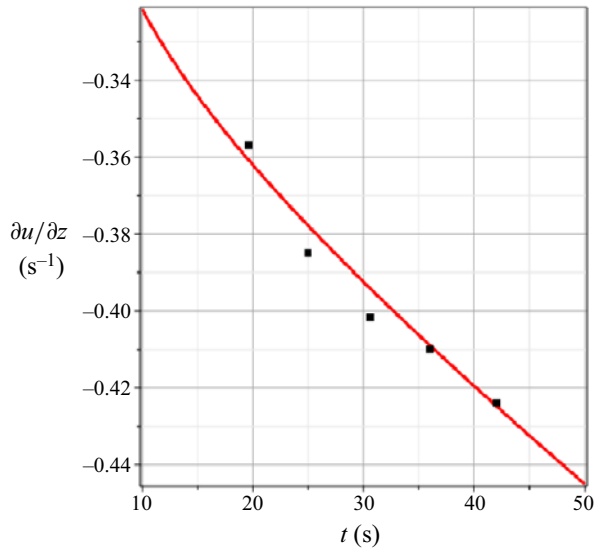
Figure 7. Theoretical Eulerian drift gradient at $z = \delta_1$ (red line) as a function of time. Here, $u = u_{E1} + u_{R1}$ from (2.10) and (5.3). Black squares denote value of the Lagrangian drift gradient estimated from the measurements near the interfacial boundary layer in figure 4 after $t = 19.6$, 25, 30.6, 36 and 42 s, corresponding to periods 1, 3, 5, 7, 9.

wave tank, with impermeable walls at both ends, induces a mean horizontal return flow in both layers. By correcting for the return flow in terms of mass conservation in each layer, the theoretical and laboratory results for the Lagrangian mean flow correspond quite well. Good fit is obtained for the drift gradients outside the viscous boundary layer. This is a laboratory demonstration of the effect of the VWS in producing a jet-like particle drift near the interface in a two-layer system. To the authors' knowledge, the transient Eulerian response to the VWS has not been observed in the laboratory before.

Oil on water is commonly observed in nature, from monomolecular films to much thicker layers (Alofs & Reisbig 1972; Lange & Hühnerfuss 1978). In the latter case, the presence of an oil spill is usually related to shipwrecking or accidents at offshore oil installations. Future offshore oil explorations are expected to move towards shallow Arctic regions where sea ice is present, at least for part of the year. In this case, accidental release of oil may be particularly difficult to handle in the presence of waves. Generally, ocean swell originates in the open sea and propagates towards the ice front, or the marginal ice zone; suffering increased attenuation as it moves further into the ice-covered region; see e.g. Squire & Moore (1980). As we have shown in this paper, long gravity waves on the oil/water boundary may induce a net transport oil further into the region beneath the ice. This net transport is much larger than the traditional Stokes drift. Obviously, it will complicate any oil recovery operation.

Finally, the uncertainty related to the theoretical parameterization of the return flow in a closed tank should not over-shadow the obvious need for more careful measurements near the wave generator and at the far end of the tank in order to reveal the nature of the return flow.

Declaration of interests. The authors report no conflict of interest.

Author ORCIDs.

Ⓓ Jan Erik H. Weber http://orcid.org/0000-0002-2310-3649;

Ⓓ Jean Rabault http://orcid.org/0000-0002-7244-6592;

Ⓓ Atle Jensen http://orcid.org/0000-0001-7376-0850.

REFERENCES

ALOFS, D.J. & REISBIG, R.L. 1972 An experimental evaluation of oil slick movement caused by waves. *J. Phys. Oceanogr.* **2**, 439–443.

CHRISTENSEN, K.H. & WEBER, J.E.H. 2005 Drift of an inextensible sheet caused by surface waves. *Environ. Fluid Mech.* **5**, 492–505.

CRAIK, A.D.D. 1982 The drift in water waves. *J. Fluid Mech.* **116**, 187–205.

DALZIEL, S.B. 2006 *Digiflow User Guide, Version 1*. DL Research Partners.

DORE, B.D. 1970 Mass transport in a layered fluid system. *J. Fluid Mech.* **40**, 113–126.

DORE, B.D. 1973 On mass transport induced by interfacial oscillations at a single frequency. *Proc. Camb. Phil. Soc.* **74**, 333–347.

DORE, B.D. 1978*a* Some effects of the air-water interface on gravity waves. *Geophys. Astrophys. Fluid Dyn.* **10**, 215–230.

DORE, B.D. 1978*b* A double boundary-layer model of mass transport in progressive interfacial waves. *J. Engng Maths* **12**, 289–301.

GRUE, J., JENSEN, A., RUSAS, P.O. & SVEEN, J.K. 2000 Breaking and broadening of internal solitary waves. *J. Fluid Mech.* **413**, 181–217.

LANGE, P. & HÜHNERFUSS, H. 1978 Drift response of monomolecular slicks to wave and wind action. *J. Phys. Oceanogr.* **8**, 142–150.

LONGUET-HIGGINS, M.S. 1953 Mass transport in water waves. *Phil. Trans. R. Soc. Lond.* A **245**, 535–581.

LONGUET-HIGGINS, M.S. 1969 A nonlinear mechanism for the generation of sea waves. *Proc. R. Soc. Lond.* A **311**, 371–389.

NG, C.-O. 2004 Mass transport and set-ups due to partial standing surface waves in a two-layer viscous system. *J. Fluid Mech.* **520**, 297–325.

PIEDRA-CUEVA, I. 1995 Drift velocity of spatially decaying waves in a two-layer viscous system. *J. Fluid Mech.* **299**, 217–239.

PIROLT, J.A. 2021 Drift and generation of interfacial progressive waves in immiscible fluids. Master thesis, Department of Mathematics, University of Oslo.

RABAULT, J., HALSNE, T., SUTHERLAND, G. & JENSEN, A. 2016 PTV investigation of the mean drift currents under water waves. In *18th International Symposium on the Application of Laser and Imaging Techniques to Fluid Mechanics*.

SAKAKIYAMA, T. & BYKER, E.W. 1989 Mass transport velocity in mud layer due to progressive waves. *ASCE J. Waterway Port Coastal Ocean Engng* **115**, 614–633.

SQUIRE, V.A. & MOORE, S.C. 1980 The attenuation of ocean waves in the marginal ice zone. *Nature* **283**, 365–368.

STOKES, G.G. 1847 On the theory of oscillatory waves. *Trans. Camb. Phil. Soc.* **8**, 441–455.

TROY, C.D. & KOSEFF, J.R. 2006 The viscous decay of progressive interfacial waves. *Phys. Fluids* **18**, 026602.

UMEYAMA, M. & MATSUKI, S. 2011 Measurements of velocity and trajectory of water particle for internal waves in two density layers. *Geophys. Res. Lett.* **38**, L03612.

WEBER, J.E.H. 2001 Virtual wave stress and mean drift in spatially damped surface waves. *J. Geophys. Res. Oceans* **106**, 11653–11657.

WEBER, J.E.H. & CHRISTENSEN, K.H. 2019 Virtual wave stress and transient mean drift in spatially damped long interfacial waves. *Eur. J. Mech.-B/Fluids* **77**, 162–170.

WEBER, J.E.H., CHRISTENSEN, K.H. & BROSTRÖM, G. 2014 Stokes drift in internal equatorial Kelvin waves; continuous stratification versus two-layer models. *J. Phys. Oceanogr.* **44**, 591–599.

WEBER, J.E.H. & FØRLAND, E. 1990 Effect of air on the drift velocity of water waves. *J. Fluid Mech.* **218**, 619–640.

WEN, J. & LIU, P.L.-F. 1995 Mass transport of interfacial waves in two-layer fluid system. *J. Fluid Mech.* **297**, 231–254.